

Non-isothermal crystallization behaviors and spherulitic morphology of poly(lactic acid) nucleated by a novel nucleating agent

Chenglang Li¹ · Qiang Dou¹ · Zhifei Bai¹ · Quliang Lu²

Received: 11 July 2014 / Accepted: 26 March 2015 / Published online: 10 April 2015
© Akadémiai Kiadó, Budapest, Hungary 2015

Abstract The effect of cadmium phenylmalonate (PMA-Cd) as a novel nucleating agent on the crystallization behaviors and spherulitic morphology of poly(lactic acid) (PLA) as well as non-isothermal crystallization kinetics of the nucleated PLA were studied by means of differential scanning calorimetry and polarized light microscopy. The results showed that PMA-Cd served as an effective nucleating agent to accelerate the crystallization rate of PLA. The presence of PMA-Cd significantly increased the number and decreased the size of the spherulites. The non-isothermal crystallization kinetics of the nucleated PLA was well described by Mo's model. The activation energies (ΔE) of non-isothermal crystallization were calculated by Kissinger's method. The crystallization rate of PLA/0.5 % PMA-Cd sample was faster than that of PLA/0.2 % PMA-Cd sample, while the ΔE of the former was greater than that of the latter. The nucleation mechanism between PMA-Cd and PLA was satisfactorily explained by dimensional lattice-matching criterion.

Keywords Poly(lactic acid) · Nucleating agent · Crystallization · Morphology · Non-isothermal crystallization kinetics

Introduction

With the increasing environmental problems around the world and the diminishing petroleum resources, biodegradable polymers have attracted more and more interests. Among biodegradable polymers, poly(lactic acid) (PLA) plays a special role, which is known for high mechanical properties, good biodegradability, biocompatibility, and easy forming process [1–4]. PLA is a linear aliphatic thermoplastic polyester, produced from lactic acid that is derived from renewable resources such as corn, potato, and sugar beet [4, 5]. It has been widely applied in medical apparatus, textiles, food packages, and automotive interiors, as well as agricultural materials [6–8]. However, PLA exhibits a rather slow crystallization rate, which greatly limits the practical applications. Thus, it is necessary to improve the crystallization rate of PLA to adapt for various applications. In general, blending with a nucleating agent is the most effective method to increase the crystallization rate. The nucleation activation energy is decreased, and the crystallization is initiated at higher temperature upon cooling by a nucleating agent [9–11].

Some inorganic compounds have been widely used to increase the overall crystallization rate of PLA. Li et al. [12] found that the nucleation density of PLA increased, and the crystallization half-time reduced with the addition of talc. Xiao et al. [13] also reported that the incorporation of talc increased the crystallization rate and decreased the crystallization half-time of PLA. Tábi et al. [14] found that the combination of nucleating agent (talc) and plasticizer (polyethylene glycol) had a synergistic effect on the crystallization behavior of PLA. Sun et al. [15] found that the crystallization rate of PLA increased when 3 % carbon black (CB) or modified CB was added. Kim et al. [16] and Xu et al. [17] reported that multi-walled carbon nanotube

✉ Qiang Dou
douqiang.njut@163.com

¹ College of Materials Science and Engineering, Nanjing Tech University, Nanjing 210009, China

² College of Chengxian, Southeast University, Nanjing 210088, China

(MWCNT) reduced the crystallization half-time and increased the nucleation density of PLA. Zhao et al. [18] found that the overall cold crystallization rate of PLA increased with the carboxyl functionalized MWCNTs content in PLA matrix. Wu et al. [19] found that clay increased the crystallization rate and crystallinity of PLA under the non-isothermal condition.

The stereocomplex of PLLA and PDLA was regarded as a potential nucleating agent for PLA. Tsuji and Tezuka [20] found that the overall crystallization rate of PLLA/PDLA (1:1) stereocomplexes was higher than that of pure PLLA or PDLA. Schmidt and Hillmyer [21] investigated the isothermal and non-isothermal crystallization behavior of PLLA blended with PDLA or talc. They found that the nucleation efficiency of 6 % stereocomplex was almost twice as much as that of talc. Yamane and Sasai [22] also found that the crystallization rate of PLLA increased with the addition of high molecular weight PDLA.

Recently, much attention was focused on organic compounds. Kawamoto et al. [23, 24] synthesized a series of hydrazide compounds and found that octamethylenedicarboxylic dibenzoylhydrazide (OMBH) was the most effective to accelerate the crystallization of PLA under higher cooling rate. Li and Dou [25] confirmed that OMBH was an effective nucleating agent for PLA, and the spherulitic size decreased, and the crystallinity increased for the nucleated PLA. Meanwhile, Fan et al. [26] also found that N,N'-bis(benzoyl)sebacic acid dihydrazide (BSAD) significantly improved the crystallization rate of PLA. Song et al. [27] investigated the isothermal and non-isothermal crystallization behaviors of PLA doped with a multiamide compound (TMC-328). Harris and Lee [28] found the crystallization rate and crystallinity of PLA significantly increased with the addition of ethylenebisstearamide (EBS). Pan et al. [29] found that the nucleation density of PLA increased, and the spherulitic size and the crystallization half-time reduced with the presence of uracil. Wang et al. [30] and Pan et al. [31] reported that layered metal phosphonates accelerated the crystallization rate of PLA. He et al. [32] reported that the incorporation of phthalimide could significantly improve both the non-isothermal and isothermal crystallization of PLA even at very low content. Song et al. [33] found that the non-isothermal and isothermal crystallization rates of PLA increased with zinc citrate complex nanoparticles (ZnCC) content. Li and Dou [34, 35] found that dilithium hexahydrophthalate and dilithium cis-4-cyclohexene-1,2-dicarboxylate are novel and efficient nucleating agents for PLA.

In this study, cadmium phenylmalonate (PMA-Cd) was synthesized and evaluated as a novel nucleating agent for PLA. PLA/PMA-Cd samples were prepared by melt blending. Our study was mainly focused on the non-isothermal crystallization behaviors and spherulitic morphology of the nucleated PLA.

Experimental

Materials

The commercial PLA in pellet form (4032D, 99 % L-isomers, density: 1.25 g cm^{-3} , weight average molecular weight: 207 kDa, polydispersity: 1.74, Nature Works, USA) was commercially obtained. Cadmium phenylmalonate (PMA-Cd) was synthesized by neutralization of phenylmalonic acid (PMA, analytical grade) with cadmium hydroxide (analytical grade) in our laboratory.

Fourier transform infrared spectroscopy (FTIR) characterization

The FTIR spectra of PMA and PMA-Cd were recorded with a FTIR spectrometer (Nexus 670, Thermo-Nicolet, USA) using KBr pellets over the range from 4000 to 400 cm^{-1} .

Scanning electron microscopy (SEM) observation

A SEM (JSM-6510, JEOL, Japan) was used to investigate the morphology of PMA-Cd. Before measurement, the surface of the sample was coated with a thin layer of gold.

X-ray diffraction (XRD) characterization

XRD diffraction pattern of PMA-Cd was recorded in an X-ray diffractometer (ARL X'TRA, Thermo Electron Corp., USA) using Cu K_{α} radiation ($\lambda = 0.154 \text{ \AA}$). Radial scans of intensity versus diffraction angle (2θ) were recorded in the range of 5° – 60° with a scanning rate of $5^{\circ} \text{ min}^{-1}$.

Preparation of samples

PLA pellets and PMA-Cd (0.2 and 0.5 mass% based on PLA) were dried under vacuum at 85°C for 8 h before use. Then they were mixed in an internal mixer (HL200, Jilin University Science & Technology Equipment Factory, Changchun, China) at 185°C and 40 rpm for 6 min. The melt was cooled and cut into small pieces.

A small piece was placed between two glass slides on a hot stage kept at 200°C for 5 min to make the sample melt completely and remove thermal history. It was squeezed on the top slide to form a film and then was quickly transferred onto a hot stage kept at 110°C for 60 min. The thickness of the samples after isothermal crystallization was about 0.5 mm for differential scanning calorimetry (DSC) measurement and 10- to 20- μm thickness for polarized light microscopy (PLM) observation, respectively.

DSC measurement

The melting and crystallization behaviors of the isothermally crystallized samples were performed in a differential scanning calorimeter (DSC ZF-DSC-D2, Shanghai Zufa Industry Co., Ltd., Shanghai, China) under a dry nitrogen atmosphere. The temperature and heat flow were calibrated with indium, tin, and zinc, respectively. All the samples were heated from room temperature to 200 °C at a rate of 10 °C min⁻¹ and held at 200 °C for 5 min to eliminate the thermal history. Then the melted samples were cooled down to 30 °C at a rate of 5 °C min⁻¹ and held at 30 °C for 5 min and finally reheated to 200 °C at the rate of 10 °C min⁻¹.

The melting and cooling curves of the isothermally crystallized samples were recorded. The cold crystallization temperatures (T_{cc}), melting temperature (T_m), and enthalpies of cold crystallization (ΔH_{cc}) and melting (ΔH_m) were determined from the melting curves. The onset (T_c^{on}) and peak (T_c^p) crystallization temperatures and enthalpy of crystallization (ΔH_c) were determined from the cooling curves. The total percent crystallinity (X_c) of the samples was calculated using Eq. (1).

$$X_c = \frac{\Delta H_m - \Delta H_{cc}}{\Delta H_m^0 w_{pla}} \times 100 \% \quad (1)$$

where w_{pla} is the mass% of PLA in the blend, $\Delta H_m^0 = 93.6 \text{ J g}^{-1}$ for 100 % crystalline PLA [36].

During the non-isothermal crystallization kinetics measurement, about 6 mg of each sample was sealed into an aluminum crucible, heated from 30 to 200 °C at 10 °C min⁻¹, and held at 200 °C for 5 min to remove the thermal history and then cooled to 30 °C at the constant cooling rate of 3, 6, 9, and 12 °C min⁻¹, respectively.

PLM observations

Spherulitic morphologies of the isothermally crystallized samples were observed in a polarized light microscope (LW-200-4JS, Shanghai LW Scientific Co., Ltd., Shanghai, China) equipped with cross-polars and a CCD camera. Pictures were captured and stored in a computer.

Results and discussion

Characterization of PMA-Cd

The FTIR spectra of PMA and PMA-Cd, SEM image, and XRD spectrum of PMA-Cd are shown in Fig. 1. In Fig. 1a, the characteristic absorption bands related to carboxyl (COOH) group of PMA were ν (C=O) at 1705 cm⁻¹, δ (OH) at 1396 and 931 cm⁻¹, and ν (C-O) at 1294, 1192,

and 1158 cm⁻¹. The characteristic absorption bands of PMA-Cd were ν_{as} (COO⁻) at 1580 and 1541 cm⁻¹, ν_s (COO⁻) at 1410, 1362, 1284 cm⁻¹. Obviously, the reaction product in this study was PMA-Cd.

In Fig. 1b, PMA-Cd particles exhibited the regular acicular structures. The diameter was below 1 μm , and the length was about 10 μm . Some tiny particles and agglomerates could also be found.

The XRD spectrum of PMA-Cd is shown in Fig. 1c, and the unit cell parameters calculated by the computer program TREOR90 are listed in Table 1. The crystal structure of PMA-Cd was cubic system with $a = b = c = 1.048 \text{ nm}$ and $\alpha = \beta = \gamma = 90^\circ$.

DSC measurement

Figure 2 shows the DSC melting and cooling curves of the isothermally crystallized samples, and the relevant parameters are listed in Table 2. There were double melting peaks in the first melting curves for all samples (Fig. 2a). The peak at lower temperature should be associated with the fusion of the crystals grown by normal primary crystallization, whereas the peak at higher temperature was attributed to the melting peak of the perfect crystals after reorganization during the heating process in DSC measurement [37, 38]. And the lower temperature peaks of the nucleated PLA samples were more pronounced than that of the pure PLA.

In the second melting curves (Fig. 2b), double melting peaks retained for the pure PLA and the lower temperature peak weakened, but a big cold crystallization peak appeared, indicating that the polymer chains did not fully crystallize during the cooling process. Compared with the pure PLA, the second melting curves of the nucleated PLA samples had single sharp melting peaks, due to perfect crystals formed under cooling. X_c of the nucleated PLA sample was significantly greater than that of the pure PLA. The first and second heating curves were different because of the different thermal history that the samples suffered.

In the cooling curves (Fig. 2c), no obvious crystallization peak was observed for the pure PLA, which showed that the crystallization rate of pure PLA was very slow. With the addition of the nucleating agent, the sharp crystallization peaks appeared and they shift to higher temperatures with PMA-Cd content. Moreover, ΔH_c of PLA/0.5 % PMA-Cd was greater than that of PLA/0.2 % PMA-Cd. This meant that PMA-Cd was a good nucleating agent for PLA.

PLM observations

Figure 3 shows PLM micrographs of the isothermally crystallized samples. As can be seen in Fig. 3a, the pure

Fig. 1 Characterization of PMA-Cd. **a** FTIR spectrum. **b** SEM image. **c** XRD spectrum

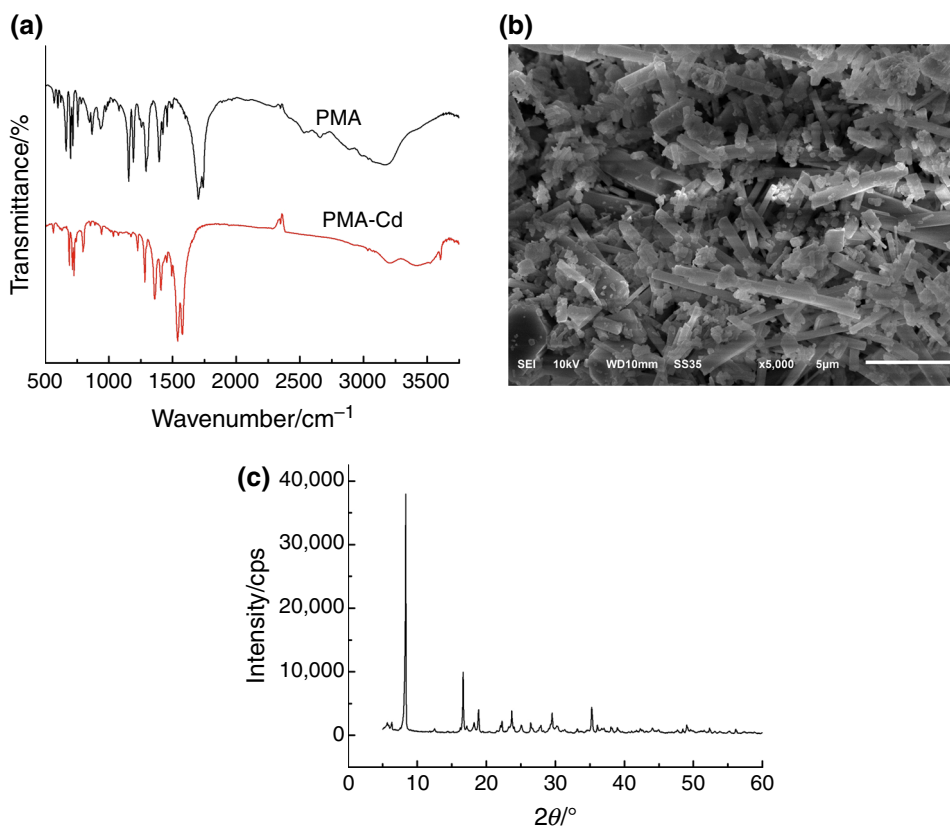


Table 1 Unit cell parameters of PMA-Cd and α -form PLA

Sample	System	a/nm	b/nm	c/nm	$\alpha/^\circ$	$\beta/^\circ$	$\gamma/^\circ$
PMA-Cd	Cubic	1.048	1.048	1.048	90	90	90
α -PLA	Orthorhombic	1.066	0.616	2.888	90	90	90

PLA sample exhibited perfect Maltase extinction crosses with the spherulitic size of roughly $100\ \mu\text{m}$, and the number was low.

With the addition of 0.2 % PMA-Cd (Fig. 3b), the Maltase extinction crosses disappeared, the spherulitic size was much smaller, and the number was huge. This indicated that PMA-Cd acted as an effective nucleating agent to induce a great number of heterogeneous nuclei; thus, many very small spherulites filled in a limited space. Moreover, the spherulitic size further decreased with addition of 0.5 % PMA-Cd (Fig. 3c), and the spherulitic size was so fine that it was hard to be figured out. Similar results were reported by Song et al. [27] and Pan et al. [29] in PLA samples nucleated with TMC-328 and EBS, respectively. The results further confirmed that the nucleation and crystallization of the nucleated PLA were greatly improved, which was in accordance with the aforementioned DSC results.

Non-isothermal crystallization behaviors of the nucleated PLA samples

Non-isothermal crystallization curves of the nucleated PLA samples at different cooling rates are shown in Fig. 4, T_c^{on} and T_c^{p} values are listed in Table 3. As the cooling rate increased, the exothermic curves of all samples became wider and shifted to lower temperatures. When the cooling rate increased from 3 to $12\ ^\circ\text{C}\ \text{min}^{-1}$, T_c^{p} of PLA/0.2 % PMA-Cd and PLA/0.5 % PMA-Cd decreased from 130.6 and $132.9\ ^\circ\text{C}$ to 115.2 and $117.1\ ^\circ\text{C}$, respectively. The rearrangement of polymer chains into the lattices was a relaxation process; a certain time was required to complete this process. At a lower cooling rate, polymer chains had enough time to transfer from the melt to the surfaces of the crystals, so crystallization started and completed at higher temperatures. At a given cooling rate, T_c^{on} and T_c^{p} values of PLA/0.5 % PMA-Cd were greater than those of PLA/0.2 % PMA-Cd, indicating that the crystallization of PLA/0.5 % PMA-Cd started earlier than that of PLA/0.2 % PMA-Cd. This implied that PMA-Cd as a nucleating agent could accelerate the crystallization rate of PLA.

In the non-isothermal crystallization process, the relative crystallinity X_t as a function of crystallization temperature T can be expressed as:

Fig. 2 DSC curves of the isothermal crystallization samples. **a** First heating. **b** Second heating. **c** Cooling

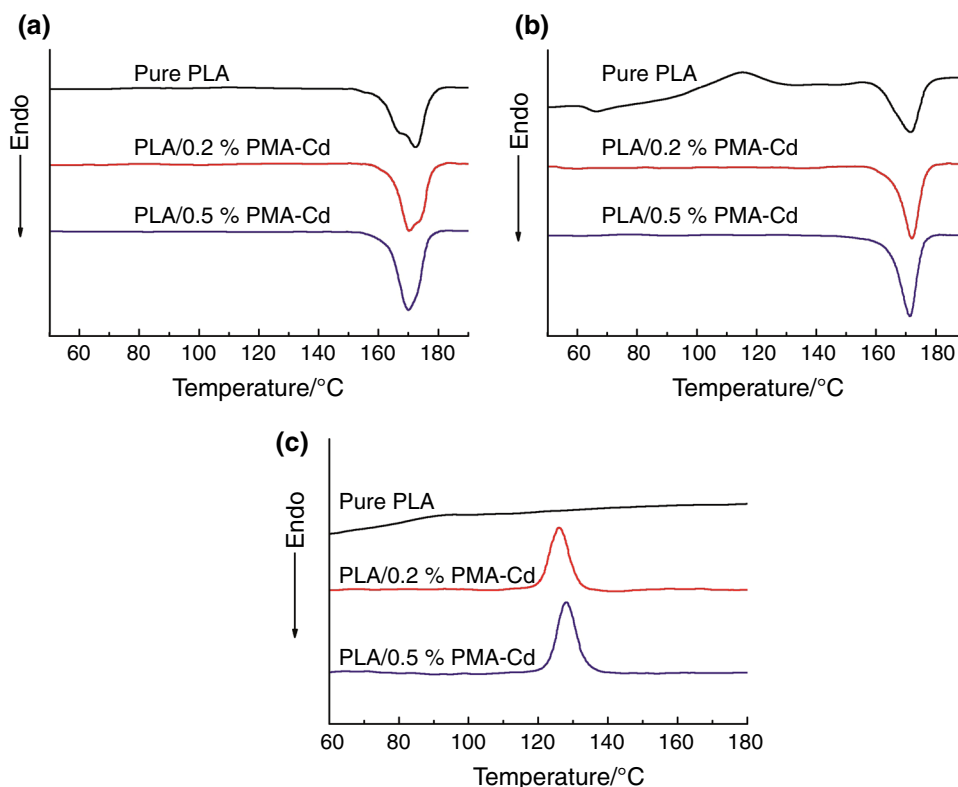


Table 2 DSC parameters of the isothermal crystallization samples

PMA-Cd/%	First heating		Second heating		Cooling	
	$T_m/^\circ\text{C}$	$T_{cc}/^\circ\text{C}$	$T_m/^\circ\text{C}$	$X_c/\%$	$T_c^p/^\circ\text{C}$	$\Delta H_c/\text{J g}^{-1}$
0	166.8, 172.1	115.4	165.2, 171.8	4.0	–	–
0.2	170.1, 172.3	–	172.1	45.4	126.1	45.2
0.5	169.8, 171.2	–	171.3	47.9	127.8	47.3

$$X_t = \int_{T_0}^T \left(\frac{dH_c}{dT} \right) dT / \int_{T_0}^{T_\infty} \left(\frac{dH_c}{dT} \right) dT \quad (2)$$

where T_0 , T , and T_∞ are the initial, arbitrary, and final crystallization temperatures, respectively. X_t —temperature curves of the nucleated PLA are presented in Fig. 5. All X_t —temperature curves showed reverse S-curves. The crystallization temperature during cooling can be converted to crystallization time:

$$t = (T_0 - T) / \Phi \quad (3)$$

where T is the temperature at time t , T_0 is the initial temperature, and Φ is the cooling rate. The transformation from T to t can be performed using a constant heating rate Φ .

Figure 6 shows X_t versus time of the nucleated PLA. All X_t —time curves exhibited typical S-curves. The crystallization half-time ($t_{1/2}$) is the crystallization time with 50 % relative crystallinity that can be obtained from Fig. 6 and is

listed in Table 3. For all samples, $t_{1/2}$ decreased with the cooling rate, indicating crystallization rate increased with the cooling rate. When the cooling rate increased from 3 to 12 °C min⁻¹, $t_{1/2}$ of PLA/0.2 % PMA-Cd and PLA/0.5 % PMA-Cd decreased from 3.00 and 2.93 min to 1.15 and 1.03 min, respectively. Furthermore, $t_{1/2}$ of PLA/0.2 % PMA-Cd was greater than that of PLA/0.5 % PMA-Cd at a given cooling rate, which suggested that the addition of more nucleating agent led to faster crystallization rate. This result was in accordance with the trend of crystallization temperatures shown in Table 3.

Non-isothermal crystallization kinetics

The Avrami equation can be used to analyze the isothermal crystallization kinetics of semi-polymers [39]:

$$1 - X_t = \exp(-Z_t t^n) \quad (4)$$

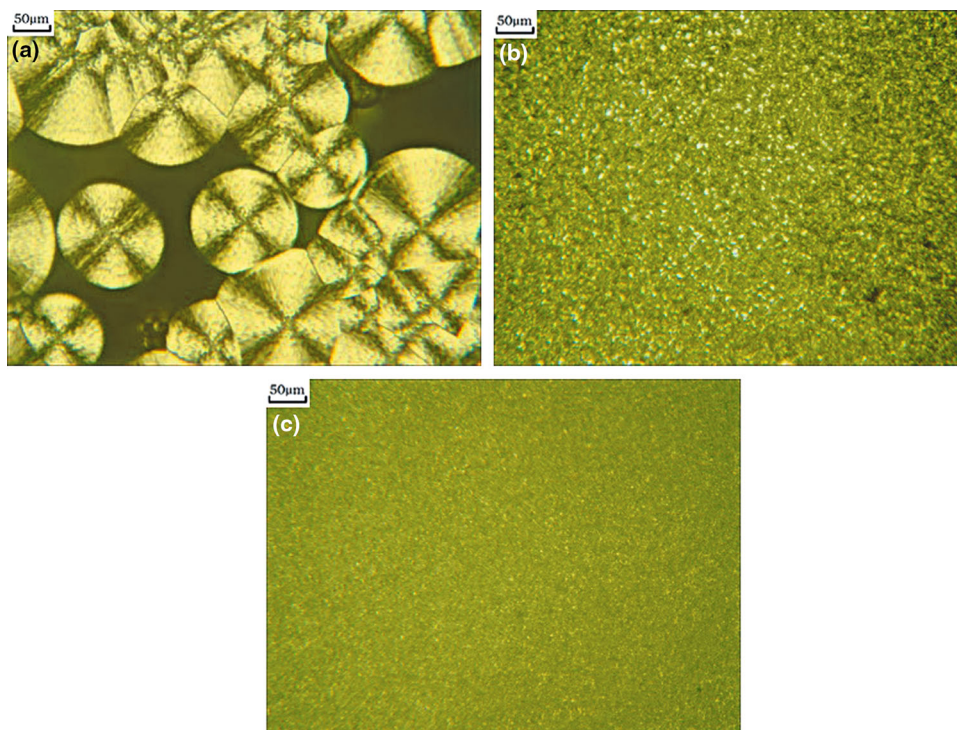


Fig. 3 PLM micrographs of the isothermal crystallization samples. **a** Pure PLA. **b** PLA/0.2 % PMA-Cd. **c** PLA/0.5 % PMA-Cd

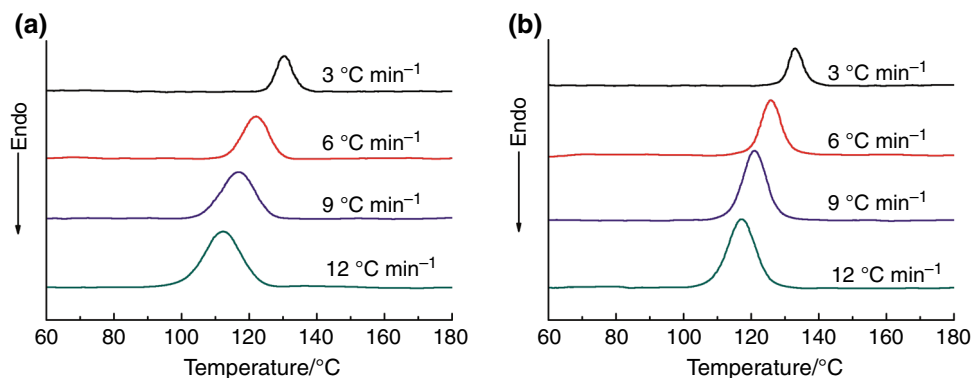


Fig. 4 Non-isothermal crystallization exotherms of the nucleated PLA samples. **a** PLA/0.2 % PMA-Cd. **b** PLA/0.5 % PMA-Cd

$$\lg[-\ln(1 - X_t)] = n \lg t + \lg Z_t \quad (5)$$

where n is the Avrami exponent, Z_t is the crystallization rate constant, and X_t is the relative crystallinity at arbitrary time t . Jeziorny [40] modified Z_t with the cooling rate Φ to analyze non-isothermal crystallization process:

$$\lg Z_c = \lg Z_t / \Phi \quad (6)$$

Assuming that the non-isothermal crystallization process was composed of infinitesimally small isothermal crystallization steps, Ozawa [41] modified the Avrami equation to describe non-isothermal crystallization process and the relative crystallinity X_t at temperature T can be calculated as follows:

$$1 - X_t = \exp(-K(T)/\Phi^m) \quad (7)$$

$$\log[-\ln(1 - X_t)] = \log K(T) - m \log \Phi \quad (8)$$

where $K(T)$ is a function of temperature, which relates to nucleation style, nucleation rate, and crystal growth rate, and m is the Ozawa exponent, which depends on the dimensions of the crystal growth.

Mo and coworkers [42, 43] developed a method by combining Avrami and Ozawa (a modified Avrami model) models to describe the non-isothermal crystallization process, as expressed in following:

$$\lg \Phi = \lg F(T) - \alpha \lg t \quad (9)$$

Table 3 Non-isothermal crystallization parameters of the nucleated PLA samples

Sample	$\Phi/^\circ\text{C min}^{-1}$	$T_c^{on}/^\circ\text{C}$	$T_c^p/^\circ\text{C}$	$t_{1/2}/\text{min}$
PLA/0.2 % PMA-Cd	3	139.5	130.6	3.00
	6	131.8	122.1	1.65
	9	129.3	117.1	1.41
	12	125.8	115.2	1.15
PLA/0.5 % PMA-Cd	3	142.0	132.9	2.93
	6	137.7	125.9	1.96
	9	134.1	121.0	1.45
	12	129.4	117.1	1.03

$$F(T) = [K(T)/Z_c]^{1/m} \tag{10}$$

$$\alpha = n/m \tag{11}$$

where n is the Avrami exponent, m is the Ozawa exponent, $K(T)$ is the cooling function of crystallization temperature in Ozawa's equation, and $F(T)$ is the value of the cooling rate to be chosen at a unit crystallization time when the system has the same crystallinity. When $\lg\Phi$ is plotted versus $\ln t$, the intercept is $\lg F(T)$, and the slope is $-\alpha$. A high value of $F(T)$ means that a high cooling rate is needed to reach a certain relative crystallinity in unit crystallization time, which indicates the difficulty of the crystallization process.

Figure 7 shows the plots of $\lg\Phi$ versus $\lg t$ at different relative crystallinity of the nucleated PLA, and $F(T)$ and α are listed in Table 4. According to the values of r^2 (a measure of goodness of fit of linear regression), significant linear correlations between $\lg\Phi$ and $\lg t$ were observed for all samples, indicating that Mo's model well described the non-isothermal crystallization of the nucleated PLA. It was shown that α increased with X_t , and α of PLA/0.2 % HHPA-Li was lower than that of PLA/0.5 % PMA-Cd. $F(T)$ also increased with X_t , which suggested that higher cooling rate was needed to obtain higher X_t in unit crystallization time. When X_t increased from 20 to 80 %, $F(T)$ of PLA/0.2 % PMA-Cd and PLA/0.5 % PMA-Cd increased from 9.04 and 8.91 to 22.86 and 21.38, respectively. For the same X_t , a higher cooling rate was needed for PLA/0.2 % HHPA-Li than that of PLA/0.5 % PMA-Cd. The result showed that the crystallization rate of PLA/0.2 % PMA-Cd was slower than that of PLA/0.5 % PMA-Cd, which was in accordance with the results in Table 3. Xiao et al. [13] reported that Mo's model could satisfactorily describe the non-isothermal crystallization behavior of PLA, and $F(T)$ decreased after the addition of talc. Su et al. [15] found that Mo's model could describe non-isothermal crystallization kinetics of PLA nucleated with carbon black (CB) or modified CB. For the same X_t , $F(T)$ values of PLA/CB and PLA/modified CB were lower than that of PLA.

Fig. 5 X_t —temperature for the nucleated PLA samples. **a** PLA/0.2 % PMA-Cd. **b** PLA/0.5 % PMA-Cd

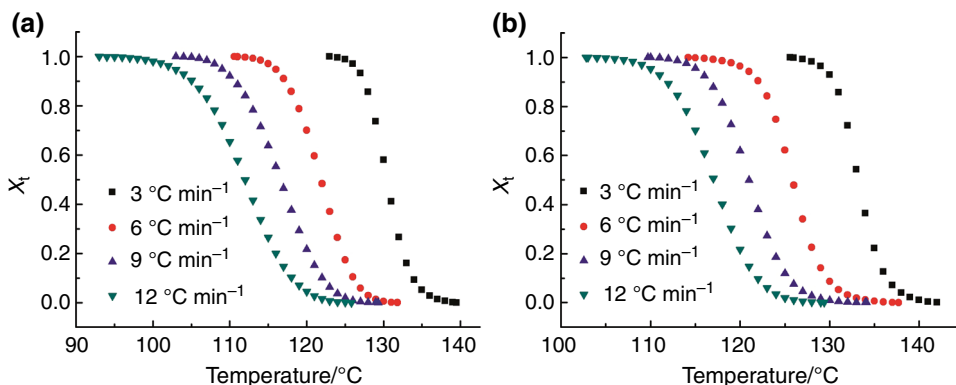


Fig. 6 X_t —time for the nucleated PLA samples. **a** PLA/0.2 % PMA-Cd. **b** PLA/0.5 % PMA-Cd

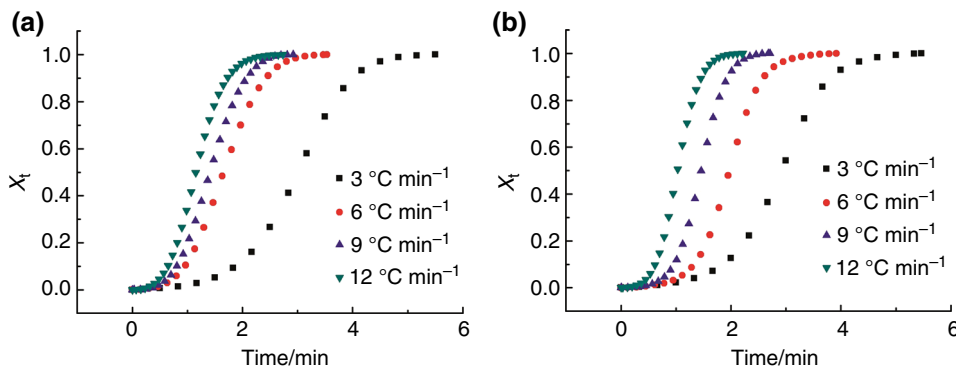


Fig. 7 $\lg\Phi$ versus $\lg t$ for the nucleated PLA samples. **a** PLA/0.2 % PMA-Cd. **b** PLA/0.5 % PMA-Cd

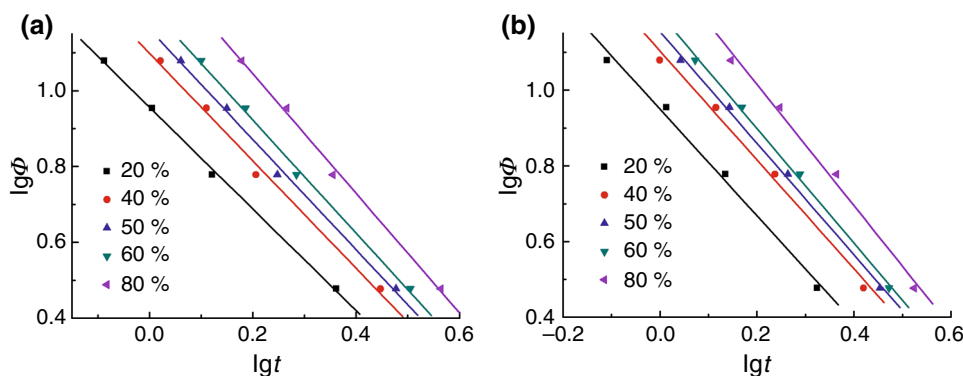


Table 4 Mo's parameters for the nucleated PLA samples

Sample	$X_d/\%$	$F(T)$	α	r^2
PLA/0.2 % PMA-Cd	20	9.04	1.34	0.9963
	40	12.59	1.42	0.9912
	50	14.52	1.45	0.9939
	60	16.59	1.49	0.9924
	80	22.86	1.58	0.9939
PLA/0.5 % PMA-Cd	20	8.91	1.41	0.9883
	40	12.53	1.44	0.9865
	50	14.13	1.48	0.9941
	60	15.85	1.51	0.9968
	80	21.38	1.60	0.9887

Crystallization activation energy

The crystallization activation energy (ΔE) is the energy required to transport molecular segments to the crystallization surfaces. Taking the influence of different cooling rate on the crystallization process into account, Kissinger [44] proposed an equation for calculating ΔE during non-isothermal crystallization process:

$$\frac{d \left[\ln \left(\frac{\Phi}{T_c^2} \right) \right]}{d \left(\frac{1}{T_c} \right)} = - \frac{\Delta E}{R} \quad (12)$$

where T_c is the peak crystallization temperature, Φ is the cooling rate, and R is the universal gas constant. ΔE can be obtained from the slope of $\ln(\Phi/T_c^2)$ versus $1/T_c$.

Figure 8 shows the plot of $\ln(\Phi/T_c^2)$ against $1/T_c$ for the non-isothermal crystallization of the nucleated PLA samples. The calculated $|\Delta E|$ of PLA/0.2 % PMA-Cd and PLA/0.5 % PMA-Cd was 105.65 and 122.39 kJ mol^{-1} , respectively, i.e., the addition of more nucleating agent led to greater $|\Delta E|$. $|\Delta E|$ is the sum of the activation energy of the nucleation and crystal growth processes. Generally, a higher $|\Delta E|$ would hinder the crystallization and result in the decrease in crystallization rate [13]. However, an

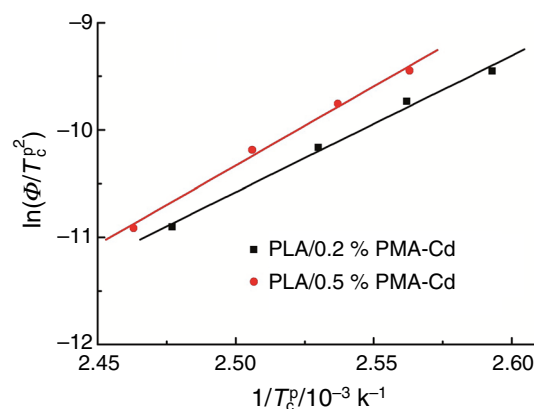


Fig. 8 Crystallization activation energy calculated from Kissinger model

opposite result was obtained in our study. The addition of more nucleating agent led to greater $|\Delta E|$, but it also increased the crystallization rate. Similar results were also found in PLA modified with functionalized MWCNTs [18] and clay [19], respectively. Presumably, the nucleating agent impeded the transportation of PLA chain segments to the crystal growth surfaces due to the strong interaction between the nucleating agent and the segments of PLA, resulting in the increase of $|\Delta E|$. The crystallization process was controlled by two processes: nucleation and spherulitic growth [45]. It seemed that in our case, the nucleation effect predominated the crystallization process and the increase in the nucleation rate led to the increase in the overall crystallization rate and crystallization temperatures.

Nucleation mechanism

The heterogeneous nucleation mechanism based on the surface free-energy consideration was first proposed to explain the nucleation effect of carboxylates in polyolefins [46–48]. The chemical nucleation mechanism was proposed in the case of chemically reactive polymers [e.g., poly(ethylene terephthalate), PET] and organic nucleating

agent system. The nucleating agent (e.g., sodium 2-chlorobenzoate) dissolved in the polymer and reacted as true chemical reagents with the molten macromolecules to form nucleating species [49, 50].

Nowadays, the epitaxial mechanism based on the dimensional lattice-matching rules prevails in this subject [51, 52]. The epitaxial nucleation mechanism was successfully applied in the polypropylene/nucleating agents [11, 53–61], PET/talc [62], poly(hydroxyl butyrate)/ammonium chloride [63], and poly[(3-hydroxybutyrate)-co-(3-hydroxyhexanoate)]/zinc phenylphosphonate [64] systems. For PLA/carboxylate nucleating agents, the chemical nucleation mechanism was abandoned and the epitaxial mechanism was adopted in PLA/zinc phenylphosphonate [31] and PLA/zinc citrate complex nanoparticle [33] systems.

Epitaxial crystallization of polymers rests on the fact that substrate and deposit have matching structural features that are repeated in the contact plane, that is, the so-called dimensional lattice-matching criterion. PLA crystallizes in three modifications (α -, β -, and γ -forms). The most common α -form occurs in conventional melt and solution crystallization conditions. The unit cell parameters of α -form PLA [65] and PMA-Cd are listed in Table 1, and the schematic crystal structures of them are shown in Fig. 9. Quantitative estimation of the matching between a period PA of a substrate and a period PB of a polymer crystal is made in terms of the misfit factor, $f_m = 100 \times (PB - PA)/PA$. Empirically, if $f_m < 15\%$, the epitaxy is regarded as good [56]. The length of a-axis of α -PLA was roughly equal to that of any axis of PMA-Cd. f_m between them was 1.7%, which showed a good matching relationship between them. It also suggested that the a-axis of α -PLA was parallel with any axis of PMA-Cd. In addition to the

matching along the $a_{\alpha\text{-PLA}}$, the lateral matching also should be checked. The f_m between the length of $c_{\alpha\text{-PLA}}$ and triple length of any axis of PMA-Cd was 8.1%, which showed that one helical period of α -PLA could be packed in three spans of any axis of PMA-Cd. Thus, any plane of PMA-Cd might be in contact with the ac-plane [i.e., (010) face] of α -PLA. The details needed more investigation. As discussed above, the crystal structures of PMA-Cd and α -PLA satisfied the lattice-matching relationship.

Conclusions

The non-crystallization behaviors and spherulitic morphologies of the pure PLA and the nucleated PLA samples as well as the non-isothermal crystallization kinetics of the nucleated PLA were investigated in this paper. DSC results indicated that PMA-Cd remarkably increased the crystallization temperatures and the crystallinities of PLA. PLM observations showed that the addition of PMA-Cd significantly decreased the size and increased the number of spherulites. The non-isothermal crystallization kinetics of the nucleated PLA samples were well described by Mo's model. The results showed that the crystallization rate of PLA/0.5% PMA-Cd sample was faster than that of PLA/0.2% PMA-Cd. In addition, the results of the Kissinger's method showed that $|\Delta E|$ increased with the nucleating agent content. A good dimensional lattice-matching relationship was realized between the crystal structures of PMA-Cd and α -PLA.

Acknowledgements The authors gratefully acknowledge the partial financial support of this work by A Project Funded by the Priority Academic Program Development of Jiangsu Higher Education Institutions (PAPD).

References

1. Drumright RE, Gruber PR, Henton DE. Polylactic acid technology. *Adv Mater*. 2000;12:1841–6.
2. Lim LT, Auras R, Rubino M. Processing technologies for poly(lactic acid). *Prog Polym Sci*. 2008;33:820–52.
3. Kim KW, Lee BH, Kim HJ, Sriroth K, Dorgan JR. Thermal and mechanical properties of cassava and pineapple flours-filled PLA bio-composites. *J Therm Anal Calorim*. 2012;108:1131–9.
4. Shi N, Dou Q. Non-isothermal cold crystallization kinetics of poly(lactic acid)/poly(butylene adipate-co-terephthalate)/treated calcium carbonate composites. *J Therm Anal Calorim*. 2015;119:635–42.
5. Amass W, Amass A, Tighe B. A review of biodegradable polymers: uses, current developments in the synthesis and characterization of biodegradable polyesters, blends of biodegradable polymers and recent advances in biodegradation studies. *Polym Int*. 1998;47:89–144.
6. Ikada Y, Tsuji H. Biodegradable polyesters for medical and ecological applications. *Macromol Rapid Commun*. 2000;21:117–32.

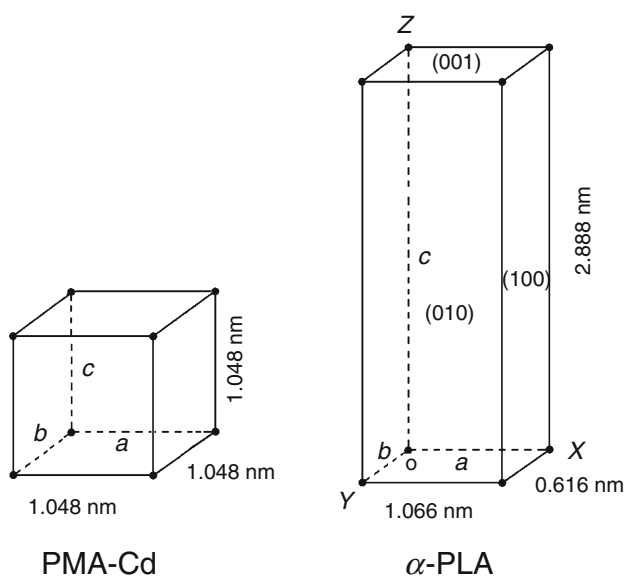


Fig. 9 Schematic crystal structures of PMA-Cd and α -form PLA

7. Martino VP, Ruseckaite RA, Jimenez A. Thermal and mechanical characterization of plasticized poly (L-lactide-co-D, L-lactide) films for food packaging. *J Therm Anal Calorim.* 2006;86:707–12.
8. Blanco I, Siracusa V. Kinetic study of the thermal and thermo-oxidative degradations of polylactide-modified films for food packaging. *J Therm Anal Calorim.* 2013;112:1171–7.
9. Li H, Huneault MA. Effect of nucleation and plasticization on the crystallization of poly(lactic acid). *Polymer.* 2007;48:6855–66.
10. Okada K, Watanabe K, Urushihara T, Toda A, Hikosaka M. Role of epitaxy of nucleating agent (NA) in nucleation mechanism of polymers. *Polymer.* 2007;48:401–8.
11. Yoshimoto S, Ueda T, Yamanaka K, Kawaguchi A, Tobita E, Haruna T. Epitaxial act of sodium 2,2'-methylene-bis-(4,6-di-*t*-butylphenylene) phosphate on isotactic polypropylene. *Polymer.* 2001;42:9627–31.
12. Li M, Hu DF, Wag YM, Shen CY. Nonisothermal crystallization kinetics of poly(lactic acid) formulations comprising talc with poly(ethylene glycol). *Polym Eng Sci.* 2010;50:2298–305.
13. Xiao H, Yang L, Ren X, Jiang T, Yeh J-T. Kinetics and crystal structure of poly(lactic acid) crystallized nonisothermally: effect of plasticizer and nucleating agent. *Polym Compos.* 2010;31:2057–68.
14. Tábi T, Suplicz A, Czígány T, Kovács JG. Thermal and mechanical analysis of injection moulded poly(lactic acid) filled with poly(ethylene glycol) and talc. *J Therm Anal Calorim.* 2014;118:1419–30.
15. Su Z, Guo W, Liu Y, Li Q, Wu C. Non-isothermal crystallization kinetics of poly (lactic acid)/modified carbon black composite. *Polym Bull.* 2009;62:629–42.
16. Kim SY, Shin KS, Lee SH, Kim KW, Youn JR. Unique crystallization behavior of multi-walled carbon nanotube filled poly(lactic acid). *Fiber Polym.* 2010;11:1018–23.
17. Xu Z, Niu Y, Wang Z, Li H, Yang L, Qiu J, Wang H. Enhanced nucleation rate of polylactide in composites assisted by surface acid oxidized carbon nanotubes of different aspect ratios. *ACS Appl Mater Interfaces.* 2011;3:3744–53.
18. Zhao Y, Qiu Z, Yan S, Yang W. Crystallization behavior of biodegradable poly(L-lactide)/multiwalled carbon nanotubes nanocomposites from the amorphous state. *Polym Eng Sci.* 2011;51:1564–73.
19. Wu D, Wu L, Wu L, Xu B, Zhang Y, Zhang M. Nonisothermal cold crystallization behavior and kinetics of polylactide/clay nanocomposites. *J Polym Sci B Polym Phys.* 2007;45:1100–13.
20. Tsuji H, Tezuka Y. Stereocomplex formation between enantiomeric poly(lactic acid)s. 12. Spherulite growth of low-molecular-weight poly(lactic acid)s from the melt. *Biomacromolecules.* 2004;5:1181–6.
21. Schmidt SC, Hillmyer MA. Polylactide stereocomplex crystallites as nucleating agents for isotactic polylactide. *J Polym Sci B Polym Phys.* 2001;39:300–13.
22. Yamane H, Sasai K. Effect of the addition of poly(D-lactic acid) on the thermal property of poly(L-lactic acid). *Polymer.* 2003;44:2569–75.
23. Kawamoto N, Sakai A, Horikoshi T, Urushihara T, Tobita E. Physical and mechanical properties of poly(L-lactic acid) nucleated by dibenzoylhydrazide compound. *J Appl Polym Sci.* 2007;103:244–50.
24. Kawamoto N, Sakai A, Horikoshi T, Urushihara T, Tobita E. Nucleating agent for poly(L-lactic acid)—an optimization of chemical structure of hydrazide compound for advanced nucleation ability. *J Appl Polym Sci.* 2007;103:198–203.
25. Li C, Dou Q. Crystallization behavior of poly(lactic acid) nucleated by a hydrazide compound. *Adv Mater Res.* 2013;710:85–8.
26. Fan Y, Yu Z, Cai Y, Hu D, Yan S, Chen X, Yin J. Crystallization behavior and crystallite morphology control of poly(L-lactic acid) through N,N'-bis(benzoyl)sebacic acid dihydrazide. *Polym Int.* 2013;2:647–57.
27. Song P, Wei Z, Liang J, Chen G, Zhang W. Crystallization behavior and nucleation analysis of poly(L-lactic acid) with a multiamide nucleating agent. *Polym Eng Sci.* 2012;52:1058–68.
28. Harris AM, Lee EC. Improving mechanical performance of injection molded PLA by controlling crystallinity. *J Appl Polym Sci.* 2008;107:2246–55.
29. Pan P, Yang J, Shan G, Bao Y, Weng Z, Inoue Y. Nucleation effects of nucleobases on the crystallization kinetics of poly(L-lactide). *Macromol Mater Eng.* 2012;297:670–9.
30. Wang S, Han C, Bian J, Han L, Wang X, Dong L. Morphology, crystallization and enzymatic hydrolysis of poly(L-lactide) nucleated using layered metal phosphonates. *Polym Int.* 2011;60:284–95.
31. Pan P, Liang Z, Cao A, Inoue Y. Layered metal phosphonate reinforced poly(L-lactide) composites with a highly enhanced crystallization rate. *ACS Appl Mater Interfaces.* 2009;1:402–11.
32. He D, Wang Y, Shao C, Zhang G, Li Q, Shen C. Effect of phthalimide as an efficient nucleating agent on the crystallization kinetics of poly(lactic acid). *Polym Test.* 2013;32:1088–93.
33. Song P, Chen G, Wei Z, Chang Y, Zhang W, Liang J. Rapid crystallization of poly(L-lactic acid) induced by a nanoscaled zinc citrate complex as nucleating agent. *Polymer.* 2012;53:4300–9.
34. Li C, Dou Q. Non-isothermal crystallization kinetics and spherulitic morphology of nucleated poly(lactic acid): effect of dilithium hexahydrophthalate as a novel nucleating agent. *Thermochim Acta.* 2014;594:31–8.
35. Li C, Dou Q. Non-isothermal crystallization kinetics and spherulitic morphology of nucleated poly(lactic acid): effect of dilithium cis-4-cyclohexene-1,2-dicarboxylate as a novel and efficient nucleating agent. *Polym Adv Technol.* 2015;26:376–84.
36. Martin O, Averous L. Poly(lactic acid):plasticization and properties of biodegradable multiphase systems. *Polymer.* 2001;42:6209–19.
37. Yasuniwa M, Tsubakihara S, Sugimoto Y, Nakafuku C. Thermal analysis of the double-melting behavior of poly(L-lactic acid). *J Polym Sci B Polym Phys.* 2004;42:25–32.
38. Song P, Chen G, Wei Z, Zhang W, Liang J. Calorimetric analysis of the multiple melting behavior of melt-crystallized poly(L-lactic acid) with a low optical purity. *J Therm Anal Calorim.* 2013;111:1507–14.
39. Avrami M. Kinetics of phase change II. Transformation-time relations for random distribution of nuclei. *J Chem Phys.* 1940; 8:212–24.
40. Jeziorny A. Parameters characterizing the kinetics of the non-isothermal crystallization of poly(ethylene terephthalate) determined by DSC. *Polymer.* 1978;19:1142–4.
41. Ozawa T. Kinetics of non-isothermal crystallization. *Polymer.* 1971;12:150–8.
42. Liu T, Mo Z, Wang S, Zhang H. Nonisothermal melt and cold crystallization kinetics of poly(aryl ether ether ketone ketone). *Polym Eng Sci.* 1997;37:568–75.
43. Liu T, Mo Z, Zhang H. Nonisothermal crystallization behavior of a novel poly(aryl ether ketone): PEDEKMK. *J Appl Polym Sci.* 1998;67:815–21.
44. Kissinger HE. Variation of peak temperature with heating rate in differential thermal analysis. *J Res Natl Bur Stand.* 1956;57: 217–21.
45. Mucha M, Królikowski Z. Application of DSC to study crystallization kinetics of polypropylene containing fillers. *J Therm Anal Calorim.* 2003;74:549–57.
46. Binsbergen FL. Heterogeneous nucleation in the crystallization of polyolefins: part 1. chemical and physical nature of nucleating agents. *Polymer.* 1970;11:253–67.
47. Binsbergen FL, De Lange BGM. Heterogeneous nucleation in the crystallization of polyolefins: part 2. kinetics of crystallization of nucleated polypropylene. *Polymer.* 1970;11:309–32.

48. Binsbergen FL. Heterogeneous nucleation in the crystallization of polyolefins. III. Theory and mechanism. *J Polym Sci Polym Phys Ed.* 1973;11:117–35.
49. Legras R, Mercier JP, Nield E. Polymer crystallization by chemical nucleation. *Nature.* 1983;304:432–4.
50. Mercier JP. Nucleation in polymer crystallization: a physical or a chemical mechanism? *Polym Eng Sci.* 1990;30:270–8.
51. Wittmann JC, Lotz B. Epitaxial crystallization of polyethylene on organic substrates: a reappraisal of the mode of action of selected nucleating agents. *J Polym Sci Polym Phys Ed.* 1981;19:1837–51.
52. Wittmann JC, Lotz B. Epitaxial crystallization of polymers on organic and polymeric substrates. *Prog Polym Sci.* 1990;15:909–48.
53. Stocker W, Schumacher M, Graff S, Thierry A, Wittmann J-C, Lotz B. Epitaxial crystallization and AFM investigation of a frustrated polymer structure: isotactic poly(propylene), β phase. *Macromolecules.* 1998;31:807–14.
54. Mathieu C, Thierry A, Wittmann J-C, Lotz B. “Multiple” nucleation of the (010) contact face of isotactic polypropylene, α phase. *Polymer.* 2000;41:7241–53.
55. Mathieu C, Thierry A, Wittmann J-C, Lotz B. Specificity and versatility of nucleating agents toward isotactic polypropylene crystal phase. *J Polym Sci B Polym Phys.* 2002;40:2504–15.
56. Kawai T, Iijima R, Yamamoto Y, Kimura T. Crystal orientation of β -phase isotactic polypropylene induced by magnetic orientation of N, N'-dicyclohexyl-2,6-naphthalenedicarboxamide. *Polymer.* 2002;43:7301–6.
57. Dou Q. A Comparison of the effects of calcium glutarate and pimelate on the formation of β crystalline form in isotactic poly(propylene). *J Macromol Sci Part B Phys.* 2008;47:127–38.
58. Dou Q, Lu Q-L. Effect of calcium malonate on the formation of β crystalline form in isotactic poly(propylene). *Polym Adv Technol.* 2008;19:1522–7.
59. Dou Q, Lu Q-L. Effect of magnesium malonate on the formation of the β crystalline form in isotactic polypropylene. *J Vinyl Addit Technol.* 2008;14:136–41.
60. Wang J, Dou Q, Chen X, Li D. Crystal structure and morphologies of polypropylene homopolymer and propylene-ethylene random copolymer: effect of the substituted 1,3,5-benzenetrisamides. *J Polym Sci B Polym Phys.* 2008;46:1067–78.
61. Lu Q, Dou Q. Effect of a novel family of N, N'-diphenyl bisamides on the formation of β crystalline form in isotactic polypropylene. *Polym J.* 2009;41:254–9.
62. Haubruge HG, Daussin R, Jonas AM, Legras R, Wittmann JC, Lotz B. Epitaxial nucleation of poly(ethylene terephthalate) by talc: structure at the lattice and lamellar scales. *Macromolecules.* 2003;36:4452–6.
63. Organ SJ, Barham PJ. Nucleation of poly(hydroxy butyrate) by epitaxy on nitrogen-containing compounds. *J Mater Sci.* 1992;27:3239–42.
64. Yu F, Pan P, Nakamura N, Inoue Y. Nucleation effect of layered metal phosphonate on crystallization of bacterial poly[(3-hydroxybutyrate)-co-(3-hydroxyhexanoate)]. *Macromol Mater Eng.* 2011;296:103–12.
65. Sasaki S, Asakura T. Helix distortion and crystal structure of the α -form of poly(L-lactide). *Macromolecules.* 2003;36:8385–90.